The molecular structure and catalytic mechanism of a quorum-quenching *N*-acyl-L-homoserine lactone hydrolase

Myung Hee Kim*, Won-Chan Choi*, Hye Ok Kang*, Jong Suk Lee*, Beom Sik Kang†, Kyung-Jin Kim‡, Zygmunt S. Derewenda§, Tae-Kwang Oh¶, Choong Hwan Lee*‖, and Jung-Kee Lee*‖

*Korea Research Institute of Bioscience and Biotechnology, Yusong, Daejon 305-600, Korea; †School of Life Science and Biotechnology, Kyungpook National University, Daegu 702-701, Korea; ‡Pohang Accelerator Laboratory, Pohang, Kyungbuk 790-784, Korea; §Department of Molecular Physiology and Biological Physics, University of Virginia, Charlottesville, VA 22908; and ¶21C Frontier Microbial Genomics and Applications Center, Korea Research Institute of Bioscience and Biotechnology, Yusong, Daejon 305-600, Korea

Edited by Harry B. Gray, California Institute of Technology, Pasadena, CA, and approved October 13, 2005 (received for review June 15, 2005)

In many Gram-negative bacteria, including a number of pathogens such as *Pseudomonas aeruginosa* and *Erwinia carotovora*, virulence factor production and biofilm formation are linked to the quorum-sensing systems that use diffusible *N*-acyl-L-homoserine lactones (AHLs) as intercellular messenger molecules. A number of organisms also contain genes coding for lactonases that hydrolyze AHLs into inactive products, thereby blocking the quorum-sensing systems. Consequently, these enzymes attract intense interest for the development of antiinfection therapies. However, the catalytic mechanism of AHL-lactonase is poorly understood and subject to controversy. We here report a 2.0-Å resolution structure of the AHL-lactonase from *Bacillus thuringiensis* and a 1.7-Å crystal structure of its complex with L-homoserine lactone. Despite limited sequence similarity, the enzyme shows remarkable structural similarities to glyoxalase II and RNase Z proteins, members of the metallo-β-lactamase superfamily. We present experimental evidence that AHL-lactonase is a metalloenzyme containing two zinc ions involved in catalysis, and we propose a catalytic mechanism for bacterial metallo-AHL-lactonases.

quorum sensing | lactonase | metalloenzyme | crystal structure

Cell-to-cell communication mediated by small diffusible molecules is a common occurrence in many bacterial species (1, 2). This phenomenon is known as quorum sensing (QS). Many Gram-negative bacteria use *N*-acyl-L-homoserine lactones (AHLs) as signaling molecules that regulate gene expression patterns that allow the bacteria to display "group behavior." Population-dependent intercellular communication regulates such vital biological functions as antibiotic production; plasmid transfer; biofilm production; and, importantly, virulence (3).

In general terms, the QS systems in the Gram-negative bacteria are made up of two components: the LuxI proteins, which constitute AHL synthases, and the LuxR proteins, which serve as AHL receptors and transcriptional regulators (3). In addition, in recent years a number of so-called quorum-quenching enzymes, which inactivate the QS messengers, and inhibitors of QS pathways have been identified in both prokaryotes and eukaryotes (2). Given that a number of plant and animal bacterial pathogens (such as several *Erwinia* species, *Pseudomonas aeruginosa* and *Xenorhabdus nematophilus*) show AHL-dependent production of virulence factors, it has been suggested that the QS system could be used as a target for therapeutic approaches (4) also using quorum quenching enzymes. Although such approaches to control human and animal pathogens still need to be carefully investigated (5), the use of heterologous expression of bacterial AHL-lactonases in plants for protection against such infections as the blight disease shows considerable promise (6).

Although some LuxR and LuxI proteins have been structurally characterized and extensively studied (7–9), the mechanism of quorum quenching enzymes is still poorly understood. The AHL-lactonase, also referred to as autoinducer inactivation (AiiA), recently identified in a *Bacillus* species (10), is one of the most intensively studied enzymes in this group. It hydrolyzes the ester bond of the homoserine lactone ring of AHLs, renders the signaling molecules incapable of binding to their target transcriptional regulators, and consequently blocks QS. The enzyme is a 250-residue-long protein with a conserved sequence motif ^{104}HXHXDH^{109} ≈ H^{169}, similar to the Zn^{2+}-binding motif of several metallohydrolases, including the glyoxalase II and arylsulfatase enzyme families, β-lactamases, and RNase Z (10–12). However, there is controversy as to whether this motif is involved in metal binding in AHL-lactonases (13, 14).

To gain insight into the structure–function relationships in this class of enzymes, we investigated the AHL-lactonase from *Bacillus thuringiensis* subsp. *kurstaki* HD263 (hereafter referred to as BTK-AiiA). We solved the crystal structures of this protein without and with a competitive inhibitor L-HSL at 2.0- and 1.7-Å resolution, respectively. The protein shows remarkable structural similarities to metallo-β-lactamases and an even closer relationship to the human glyoxalase II (15) and to the bacterial phosphodiesterase (RNase Z; ref. 12). The electron density map of the active site of the enzyme reveals a canonical dinuclear Zn^{2+} center, and the presence of the metal ions was independently verified by atomic emission spectrometry. On the basis of the crystal structures, we propose a catalytic mechanism for BTK-AiiA along with supporting mutagenesis and biochemical data.

Materials and Methods

Mutagenesis, Expression, and Purification. Mutations were introduced into BTK-AiiA by using QuikChange site-directed mutagenesis (Stratagene). All proteins had the same two-residue cloning artifact (Met and Asp) at the N termini. Expression and purification are described in detail elsewhere (16).

Enzyme Assay. Activity assay of BTK-AiiA was performed by using the substrate *N*-hexanoyl-L-homoserine lactone (C6-AHL)

Conflict of interest statement: No conflicts declared.

This paper was submitted directly (Track II) to the PNAS office.

Freely available online through the PNAS open access option.

Abbreviations: QS, quorum sensing; AHL, *N*-acyl-L-homoserine lactone; HSL, homoserine lactone; BTK-AiiA, AHL-lactonase from *Bacillus thuringiensis* subsp. *kurstaki* HD263; C6-AHL, *N*-hexanoyl-L-homoserine lactone; LC-ESI-MS, liquid chromatography electrospray ionization MS; PDB, Protein Data Bank.

Data deposition: The atomic coordinates and structure factors have been deposited in the Protein Data Bank, www.pdb.org (PDB ID codes 2BTN and 2BR6).

‖To whom correspondence may be addressed. E-mail: chlee@kribb.re.kr or jklee@kribb.re.kr.

purchased from IDR (Daejon, Korea). The substrate specificity of BTK-AiiA was assessed against a range of AHLs as well as homoserine lactone (HSL) synthesized as enantiomerically pure L-form by IDR. The enzyme activity was evaluated by a bioassay and liquid chromatography electrospray ionization MS (LC-ESI-MS). For details, see *Supporting Text*, which is published as supporting information on the PNAS web site.

LC-ESI-MS Analysis. ESI-MS was performed to analyze BTK-AiiA reaction products by using a Finnigan LCQ Advantage MAX ion trap mass spectrometer (Thermo Electron, San Jose, CA) equipped with a Finnigan electrospray source. The HPLC separations were performed on a Finnigan Surveyor Modular HPLC System (Thermo Electron; see *Supporting Text*).

Metal Ion Determination. The metal contents were determined by inductively coupled plasma atomic emission spectrometry (PerkinElmer Elan6100; see *Supporting Text*).

Crystallization and Structure Determination. The crystallization of the native and SeMet-substituted BTK-AiiA proteins is described elsewhere (16). For details on crystallization of the BTK-AiiA complexed with L-HSL, see *Supporting Text*. The data were collected on beamlines 4A and 6B of the Pohang Accelerator Laboratory, and all data were processed by using HKL2000 (17). Anomalous differences from the Se edge data were used for the initial location of the Se atoms by using SOLVE (18). Density modification and subsequent automated model building were done with the program RESOLVE (19). Model building and refinement were performed with the programs O (20) and REFMAC5 (21). The native crystal structure was solved by molecular replacement with AMORE (22) by using the partially refined model of the SeMet crystal. The structure was refined to 2.0 Å with final R_{free} and R of 23.3% and 18.3%, respectively. The complex crystal structure was solved at a 1.7-Å resolution by molecular replacement with AMORE by using the refined model of the native crystal. The refinement resulted in R_{free} and R of 22.0% and 18.1%, respectively. See *Supporting Text* and Table 1, which is published as supporting information on the PNAS web site. The atomic coordinates and structure factor amplitudes of the native BTK-AiiA and its complex with HSL have been deposited in the Protein Data Bank (PDB) under PDB ID codes 2BTN and 2BR6, respectively.

Results

Overall Structure. The refined BTK-AiiA model shows a $\alpha\beta/\beta\alpha$ sandwich fold, with the helices forming the outer solvent exposed layer surrounding a compact core made up of β sheets (Fig. 1*A*). The molecule can be subdivided into two structural quasirepeats. The N-terminal repeat (residues 1–152) contains a single mixed β sheet with seven strands (β1, residues 4–17; β2, 30–42; β3, 45–49; β4, 74–76; β5, 99–102; β6, 121–124; and β7, 148–151) and three α helices (α1, residues 83–90; α2, residues 106–110; α3, residues 125–131). There are also six short 3_{10} helices: residues 18–20, 55–57, 79–81, 94–96, 113–115, and 139–141. The C-terminal repeat (residues 153–250) consists of a single mixed β sheet containing five strands (β8, residues 155–158; β9, 161–165; β10, 173–180; β11, 183–190; and β12, 230–233) and three α helices (α4, residues 196–200; α5, residues 210–227; and α6, residues 237–240). The N- (β1β2β3β5) and C-terminal sheets (β9β10β11β12) superpose with an rms deviation of 1.34 Å (34 superimposed α carbons; Fig. 1*D*). A search conducted by using DALI (23) revealed that BTK-AiiA shows distinct structural similarities to the metallo-β-lactamases (PDB ID codes 1JJE and 1SM1; refs. 24 and 25, respectively), methyl parathion hydrolase (PDB ID code 1P9E), and human glyoxalase II (PDB ID code 1QH5; ref. 15; Fig. 1*B*). Interestingly, the BTK-AiiA structure is also very similar to the tRNA maturase RNase Z (PDB ID code 1Y44; ref. 12; Fig. 1*C*) from *Bacillus subtilis*. These similarities could not have been easily inferred from sequence alone, because the pairwise sequence identities with BTK-AiiA are very low (≈20%). The key topological features in all these enzymes are consistently preserved, although the helical content varies among the different proteins. As such, the BTK-AiiA structure constitutes, to our knowledge, the first known example of an AHL-degrading enzyme exhibiting a canonical β-lactamase fold.

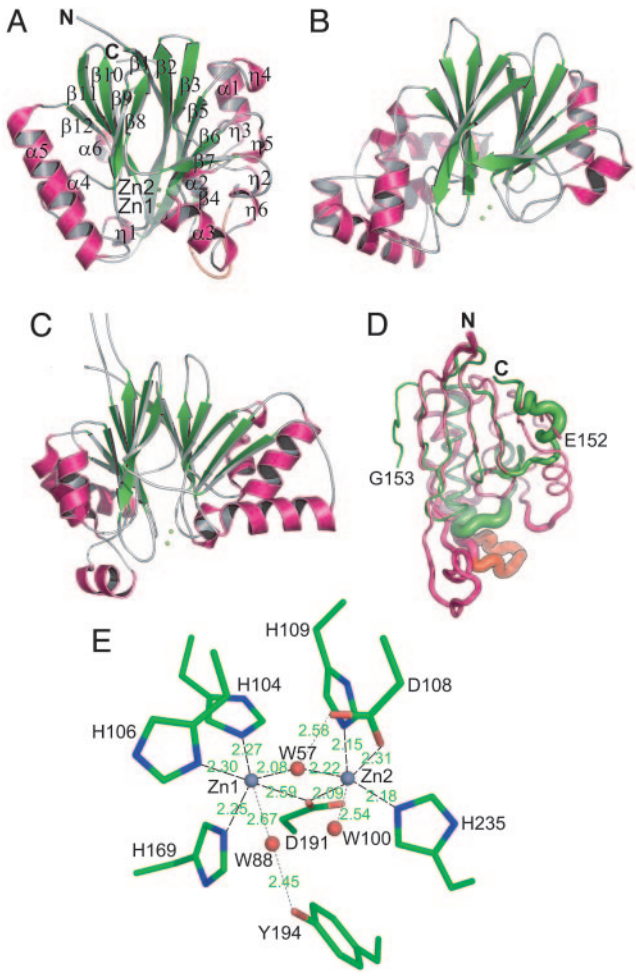

Fig. 1. Overall structure of BTK-AiiA and structural comparison of various zinc-metalloenzymes. (*A*) Ribbon representation of BTK-AiiA. α helices and β sheets are shown in purple and green, respectively. The flexible fragment of disordered electron density shown in red was stereochemically modeled by using the program O. (*B*) Human glyoxalase II (PDB ID code 1QH5) and (*C*) RNase Z (PDB ID code 1Y44) are shown. All structures are represented with two zinc ions as lime spheres in active sites. rms deviation values are 2.6 and 1.6 Å for human glyoxalase II (160 superimposed α-carbons) and RNase Z (96 superimposed α-carbons), respectively, compared with BTK-AiiA. (*D*) Superposition of the C-terminal BTK-AiiA domain in green onto the N-terminal domain in purple, colored according to temperature factors, where thicker represents higher *B* values. rms deviation is 1.34 Å for the C-terminal domain (34 superimposed α-carbons) compared with the N-terminal domain. Red loop indicates flexible fragment in BTK-AiiA. (*E*) Metal-binding center in BTK-AiiA. Interactions for metal coordination are outlined by black long-dashed lines, and hydrogen bonds are depicted as gray short-dashed lines. Interactions were measured in angstroms. Carbons, oxygens, and nitrogens are shown in green, red, and blue, respectively. Water molecules are indicated as red spheres, and zinc ions are shown as gray spheres. Unless otherwise noted, figures were prepared by using PYMOL (DeLano Scientific, South San Francisco, CA).

Dinuclear Zn^{2+}-Binding Center. Early in the refinement of the apo-enzyme, it became evident that the BTK-AiiA protein

A

Enzyme	Activity (nmol/min/mg)	
	0.1 mM zinc	0.1 mM TPEN
WT	68.6	30.2
H104A	1.0	ND
H106A	1.3	ND
D108A	1.2	ND
H109A	10.7	ND
H169A	0.8	ND
D191A	1.1	ND
D191L	0.9	ND
Y194F	22.7	8.6
H235A	10.3	ND

ND, not detectable.

B

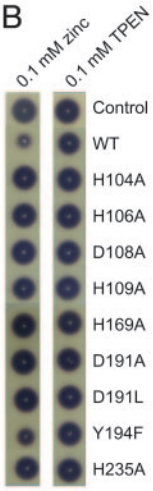

C

Enzyme	Zinc content (mol/mol of protein)	
	zinc-replenished	TPEN-treated
WT	1.88±0.02	0.18±0.01
MBP-6xHis-WT	1.92±0.03	0.16±0.03
MBP-6xHis-D108A	1.18±0.03	0.06±0.03
MBP-6xHis-H109A	0.70±0.02	0.05±0.01
MBP-6xHis-D191A	0.41±0.03	0.02±0.01
MBP-6xHis-H235A	1.09±0.02	0.12±0.04

Fig. 2. Mutagenic analysis of functional residues in the metal-binding center. (*A*) The assay was performed in the presence of 0.1 mM $ZnCl_2$ or 0.1 mM *N,N,N′, N′*-tetrakis(2-pyridylmethyl)ethylenediamine. Enzyme activity was analyzed by LC-ESI-MS. (*B*) A bioassay of enzymes was performed. Residual amounts of C6-AHL were evaluated according to the decrease in size of purple-colored areas around the hole in the CV026 plate. (*C*) The zinc contents of BTK-AiiA and its mutants. The amounts of zinc in tag-free BTK-AiiA (WT), MBP-6×His-fusion WT, and the mutant enzymes were determined by inductively coupled plasma atomic emission spectrometry, as described in *Supporting Text*.

contains a canonical dinuclear metal ion center, associated with the conserved sequence motif (^{104}HXHXDH^{109} ≈ H^{169}). Atomic emission spectrometry (see *Supporting Text*) confirmed the presence of two Zn^{2+} ions per one protein molecule (Fig. 2*C*). The ions are found at topologically equivalent positions to those observed in the metallo-β-lactamase superfamily, and the structural features of the metal-binding site are virtually identical to those of human glyoxalase II (PDB ID code 1QH5; ref. 15; Fig. 1*B*) and RNase Z (PDB ID code 1Y44; ref. 12; Fig. 1*C*). The two Zn^{2+} ions are separated by a distance of 3.4 Å and are bridged by one water molecule (or a hydroxide ion) and the Oδ2 atom of Asp-191 (Fig. 1*E*). The Zn1 ion is coordinated by His-104, -106, and -169, whereas the Zn2 ion is coordinated by His-109, His-235, and Asp-108. We note two additional water molecules present in the metal-binding center. Water molecule 88 serves as the sixth ligand for Zn1 (2.67 Å) and is also hydrogen-bonded to the hydroxyl group of Tyr-194 (2.45 Å). Water 100 serves as a ligand for the Zn2 ion (2.54 Å). Thus, each of the Zn ions shows a distorter octahedral coordination. All residues involved directly in metal coordination, as well as Tyr-194, are completely conserved in all AHL-lactonases (Fig. 6, which is published as supporting information on the PNAS web site).

Except for His-106, all histidines coordinate Zn^{2+} ions via the Nε2 atoms. An intricate network of hydrogen bonds maintains the structural integrity of the site by stabilizing side-chain conformations and ensuring that the imidazole groups present only unprotonated nitrogens to the metal ions. In the case of His-169 and -235, the side-chain conformations are stabilized by H bonds involving Nδ1 hydrogens and the main-chain carbonyls from residues 206 and 34, respectively. These bonds ensure that, under neutral pH, the imidazoles are protonated on Nδ1 and not on Nε2. Further, the conformations of His-109 and -104 are stabilized by hydrogen bonds also involving Nδ1 protons but with side chains of Asp-50 and Ser-103, respectively, as acceptors. Those residues, except for residue 206, involved in stabilization of the metal-coordination residues are completely conserved in AHL-lactonases (Fig. 6). The donor–acceptor stereochemistry is again such as to ensure deprotonation of the Nε2 atoms of the imidazoles: Asp-50 accepts one H bond from the Nδ1 of His-109 (2.91 Å) and one from the hydroxyl of Ser-103 (2.79 Å), leaving the latter poised to accept an H bond from Nδ1 of His-104 (2.89 Å). Thus, Asp-50 plays a particularly critical role by stabilizing one histidine from each of the two Zn^{2+}-binding sites. To accommodate this stereochemistry, the secondary conformation of Asp-50 is strained and falls outside the allowed region of the Ramachandran plot. The same is true of the equivalent Asp-37 in the RNase Z structure (PDB ID code 1Y44; ref. 12). Asp-112 of methyl parathion hydrolase (PDB ID code 1P9E) and Asp-29 of human glyoxalase II (PDB ID code 1QH5) also exhibit strained secondary conformations. A structurally analogous aspartate is found in the crystal structures of most metallo-β-lactamases, indicating that it may play a key role in maintaining the protein fold. To assess the functional significance of both Asp-50 and Ser-103, we mutated the former to Ser and the latter to Ala. Both mutations resulted in enzyme inactivation (data not shown), confirming their structural and functional importance.

His-106 is the only histidine that coordinates Zn^{2+} via its Nδ1 atom, not Nε2. Given that, under neutral pH, histidine is protonated preferentially on Nε2, there is less of a need for a strong H bond acceptor for this atom. Instead, the electron density map reveals a well ordered water molecule H-bonded to Nε2 of His-106. This water is also coordinated in such a way that it approaches the Nε2 with one of its free electron pairs, because its two other H bonds involve acceptor groups, i.e., Glu-136 and Tyr-137, which has its own hydroxyl proton turned to Glu-127.

To assess the functionality of the Zn^{2+}-binding residues in BTK-AiiA, we carried out a mutational analysis. Each of the zinc-coordinating residues (His-104, His-106, Asp-108, His-109, His-169, Asp-191, and His-235) was mutated to Ala, whereas Asp-191 was also mutated to Leu. The mutants were expressed and purified, and their activities were analyzed by LC-ESI-MS (Fig. 2*A*; see *Supporting Text* and Fig. 7, which is published as supporting information on the PNAS web site) and a bioassay (Fig. 2*B*; see *Supporting Text*) in the presence of 0.1 mM zinc or 0.1 mM *N,N,N′, N′*-tetrakis(2-pyridylmethyl)ethylenediamine (TPEN), that has high affinity for chelating zinc. For metal-coordinating residues, residual catalytic activity (≈15% of the native enzyme activity) was observed for the His109Ala and His235Ala mutants, whereas other mutations virtually inactivated BTK-AiiA, even in the presence of Zn^{2+}. The wild-type enzyme showed 44% of enzyme activity in the presence of 0.1 mM TPEN, suggesting that the wild-type enzyme has very high affinity for Zn^{2+} that was not removed by the chelating agent under the reaction conditions of the enzyme assay (see *Enzyme Assay* in *Supporting Text*). The same results were also observed with the bioassay. We furthermore analyzed the Zn^{2+} content of the mutant proteins (Fig. 2*C*). The molar ratios of mutant proteins D108A, H109A, and H235A to Zn^{2+} were determined to be 1.18, 0.70, and 1.09 equivalent, respectively, indicating that the mutants may be capable of binding one Zn^{2+} ion per one protein molecule. The metal content in mutant D191A was measured to be 0.41 per

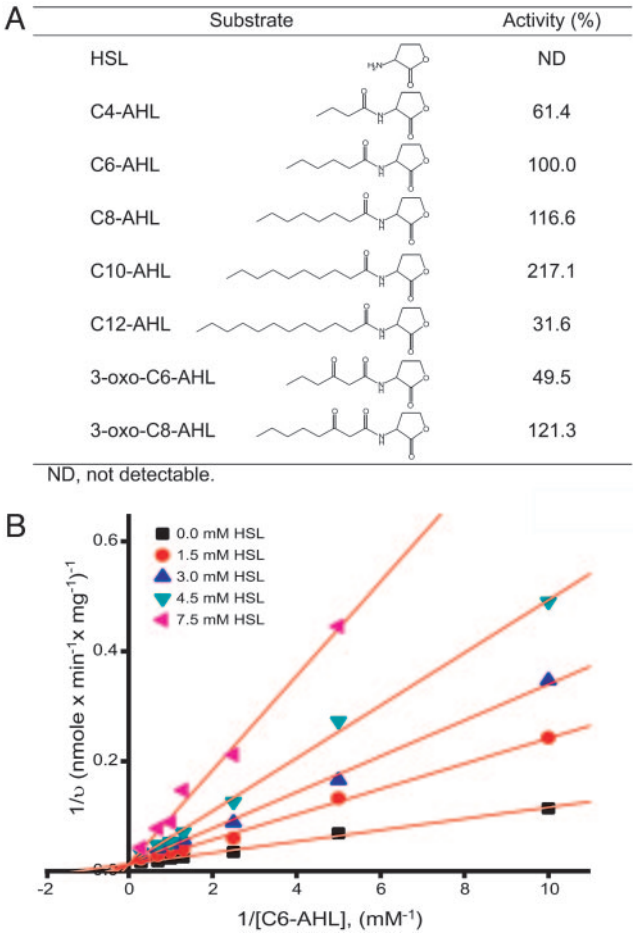

Fig. 3. Substrate specificity of BTK-AiiA and inhibition of BTK-AiiA activity by HSL. (*A*) Activity toward C6-AHL (68.6 nmol/min per mg) was defined as 100%. (*B*) A typical steady-state kinetics experiment of BTK-AiiA activity for different C6-AHL concentrations was performed at increasing concentrations of L-HSL. Enzyme activity was analyzed by LC-ESI-MS, as described in *Supporting Text*.

molecule. In the crystal structure, we see that the Oδ2 atom of Asp-191 bridges the two Zn^{2+} ions. Therefore, the D191A mutation may lead to a lower metal-binding affinity than that observed for the D108A, H109A, and H235A mutants. These results confirm that two Zn^{2+} ions are essential for the enzyme's activity.

Substrate Binding and Catalytic Mechanism. To obtain better insight into the catalytic mechanism, we thought it necessary to obtain a structure of a complex with a substrate analogue or an appropriate inhibitor. Natural acyl-HSL signals are presumed to be of the L-form, because they are biosynthesized from (*S*)-adenosyl-L-methionine, where the α-chiral center is not disturbed (9). Bioassays revealed that L-isomers were essential as the autoinducers in QS, whereas no effect was observed with D-isomers (26). *B. thuringiensis* lactonase was also reported to catalyze the hydrolysis of L-enantiomer HSL (14). Therefore, we carried out tests with various L-enantiomers of potential acyl-HSL substrates and HSL to determine the specificity of the enzyme (Fig. 3*A*). The BTK-AiiA enzyme revealed an acyl chain length preference and maximum activity with C10-AHL but was generally active against a range of acyl-HSL substrates, although not on the HSL itself. This clearly suggested that the amide linkage may be essential for proper substrate binding. We hypothesized that HSL might be a competitive inhibitor of the substrate for BTK-AiiA and therefore might compete with the substrate for the substrate-binding site on the enzyme. To investigate this possibility, the steady-state kinetics experiment of the BTK-AiiA activity for different C6-AHL concentrations was performed at increasing concentrations (0–7.5 mM) of HSL. The Lineweaver–Burk double reciprocal plots showed with straight lines that the apparent K_m values were increased, compared with the K_m of 0.74 ± 0.17 mM observed in the absence of HSL, because the HSL concentrations increased while the apparent V_{max} remained constant (Fig. 3*B*). This result demonstrates that HSL is a competitive inhibitor of AHL. The K_i value was calculated as 1.10 ± 0.39 mM. Although it has been shown that D-isomers of AHL are neither agonists nor antagonists for QS (26), we did not rule out the possibility that D-enantiomer of the HSL could be also a competitive inhibitor of AHL. We tested the possibility with D- and D,L-HSL (IDR) at a concentration of 7.5 mM. The D-isomer was similar to its inhibitory potency against C6-AHL, and consequently the racemic mixture of HSL was also inhibitory (Table 2, which is published as supporting information on the PNAS web site). Nonetheless, we cocrystallized the enzyme with L-HSL to obtain a structure more representative of the Michaelis complex. The enzyme in complex with L-HSL shows no significant conformational changes compared with the native structure with a Cα rms deviation of 0.13 Å. Residual positive electron density in the refined structure showed that HSL is bound in the catalytic site at ≈0.75 occupancy with an average *B* factor for all atoms of 34.9 Å^2 (Fig. 4*A*). The *si*-face of the lactone ring faces the zinc ions, whereas the amino group of L-HSL is positioned away from the floor of

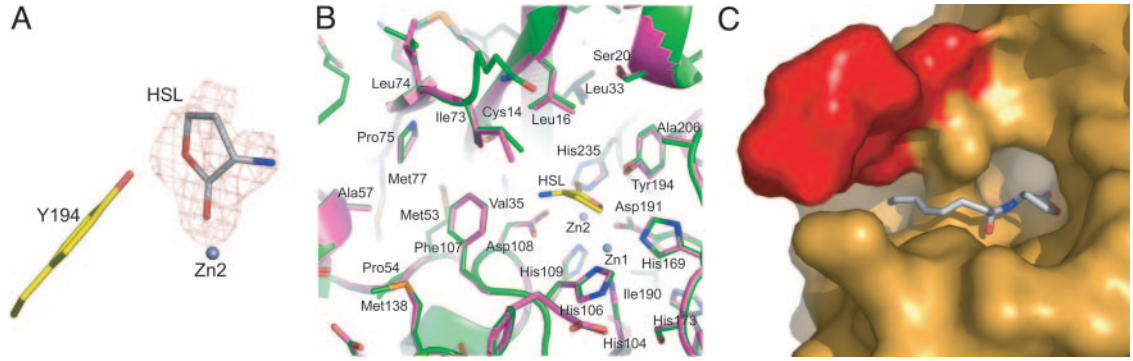

Fig. 4. Substrate binding by BTK-AiiA. (*A*) Electron density map showing the bound L-HSL in the active site of BTK-AiiA. The F_o-F_c map was calculated before the inclusion of L-HSL in the model and is contoured at 2.5 σ. (*B*) HSL-binding site and hydrophobic channel in BTK-AiiA. The hydrophobic channel is accommodated with several hydrophobic side chains and extended from the HSL-binding site. BTK-AiiA-HSL features are shown in purple, and those of the native BTK-AiiA are shown in green. HSL is shown in yellow, and zinc ions are indicated as gray spheres. (*C*) Model of AHL-binding in BTK-AiiA. The model was generated based on modeled HSL binding in BTK-AiiA by using the program O. The disordered flexible region in red was stereochemically modeled by using the program O.

the metal active center and points out toward a hydrophobic groove (see below). The carbonyl group interacts with Zn2 (2.54 Å), replacing water 100 as the metal's sixth ligand and is in close proximity of the side chain of Asp-108 (3.01 Å to Oδ1). The ring oxygen (which corresponds to the oxygen of the leaving group in the substrate) is sandwiched between Zn1 (2.44 Å) and the hydroxyl of Tyr-194 (2.45 Å), acting in the latter case as a donor in a hydrogen bond. The ring oxygen replaces water 88 as the sixth ligand of Zn1, so that in the enzyme–HSL complex, the Zn coordination is unaffected. We also note that the hydroxyl oxygen of Tyr-194 accepts a proton from the Cε-H moiety of the imidazole of His-169 (donor acceptor distance in this C—H . . . O bond is 3.09). Hydrogen bonds of the C—H . . . O type are increasingly recognized as playing important function roles in proteins (27, 28).

Assuming that the binding of the L-HSL molecule to the enzyme is representative of the substrate binding, it is possible to model the peptide linkage and the acyl chain of a canonical AHL substrate in the active site. A molecule of C8-AHL was manually docked to BTK-AiiA based on the HSL complex, using the program O (Fig. 4*C*). The acyl carbonyl fits well into a small crevice containing two backbone amide groups (residues 107 and 108), potentially donating two H bonds. It is noteworthy that in the crystal structure, these two amides are unpaired by any other H bond acceptors, which is a rare situation unless the amide plays a functional role, as is the case, for example, for hydrolytic enzymes using a so-called oxy-anion hole. We believe that the structural motif involving the 107 and 108 amides may be critical for the enzyme in that it allows binding the substrate appropriately to orient the scissile bond suitably for catalysis (see below). This would explain why HSL itself cannot be hydrolyzed and implies that *N*-formyl-L-homoserine lactone would serve as the simplest substrate.

The hydrophobic acyl chain of a natural substrate would likely fit into a crevice formed by residues Leu-16, Val-35, Met-53, Pro-54, Ala-57, Ile-73, Pro-75, Met-77, Phe-107, and Met-138 (Fig. 4*B*). The fatty acyl chain of the AHL could be laid roughly in parallel to the hydrophobic channel. In our model, residues Leu-16, Ile-73, Pro-75, Phe-107, and Met-138 made extensive van der Waals contacts with the AHL. It should be mentioned that superimposition of the native and its complex HSL structures reveals significant side-chain movements in Leu-16 and Ile-73 (Fig. 4*B*), indicating involvement of those residues in the substrate binding.

Our substrate specificity experiments (Fig. 3*A*) with BTK-AiiA yielded results that are different from those reported for the *Bacillus* sp. 240B1 AHL-lactonase (13). BTK-AiiA revealed an acyl chain length preference and maximum activity with C10-AHL, whereas the *Bacillus* sp. 240B1 AHL-lactonase had no acyl chain length preference and exhibited a broad catalytic spectrum. It is noteworthy that functional differences occur between enzymes that otherwise share 90% amino acid identity. As noted above, the crystal structure suggests which residues are involved in the acyl group binding. Of these, Ile-73 and Met-138 are replaced by Val and Leu, respectively, in the 240B1 AHL-lactonase. These sequence changes may be directly related to the different substrate specificities of the two enzymes. A replacement of Met-138 by Leu is also found in the *Bacillus* sp. COT1 AHL-lactonase (89% identity; Fig. 6). *B. thuringiensis* and *Bacillus cereus* AHL-lactonases (99% and 96% identities, respectively) show residue conservations in the predicted substrate-binding sites (Fig. 6) that may result in similar substrate preferences. However, AHL-lactonases from different genus show large variations in the amino acid sequences that may result in different substrate specificities.

The knowledge of its three-dimensional structures of BTK-AiiA with and without L-HSL and the comparison of these structures to other enzymes in the metallo-β-lactamase superfamily made it possible for us to hypothesize a catalytic pathway. We believe that the reaction follows a conserved mechanism, as described for binuclear metal-binding human glyoxalase II (15) and RNase Z (12). We specifically note that the two zinc ions are coordinated in a manner that is completely identical to that seen in RNase Z (12) with coordination ligand residues strictly conserved between both enzymes. Our proposed reaction scheme (Fig. 5) involves a nucleophilic attack by water/hydroxide bridging the two Zn^{2+} ions on the substrate's carbonyl carbon. In the structure of the complex, the nucleophilic oxygen is only 2.7 Å from the carbonyl carbon of the L-HSL, in a stereochemically ideal position for attack. The lactone ring and carbonyl oxygens of HSL interact with Zn1 and Zn2, respectively, resulting in enhanced polarization of the carbonyl bond, making it more susceptible to a nucleophilic attack. Asp-108 is suitably poised to abstract a proton, because its Oδ2 atom is only 2.5 Å from this water/hydroxide, presenting the *syn* lone electron pair. A similar mechanism has been proposed for Glu-204 in methionine aminopeptidase (29). Because the nucleophilic moiety attacks the substrate's carbonyl carbon, a negatively charged intermediate is formed, stabilized primarily by the interactions with Zn1. We believe that Tyr-194 acts as a general acid protonating the leaving group, as suggested by its strong hydrogen bond with the ring oxygen of L-HSL. To assess the role of the hydroxyl group in Tyr-194, we mutated it to a Phe. The activity indeed decreased significantly to ≈30% of the native enzyme activity (Fig. 2 *A* and *B*), in agreement with the postulated mechanism.

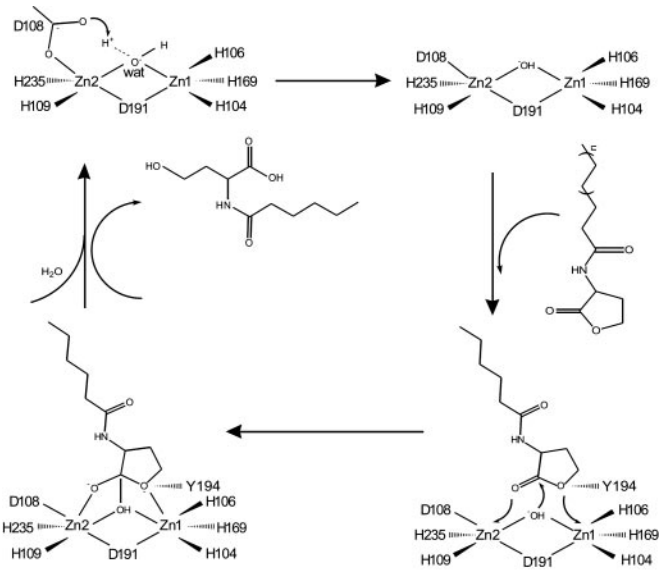

Fig. 5. Proposed catalysis mechanism for BTK-AiiA based on the BTK-AiiA–HSL complex and suggested catalysis mechanisms for other zinc metalloenzymes. See text for description.

Discussion

Since the original discovery by Dong *et al.* of an AHL-degrading enzyme from *Bacillus* sp. 240B1, there has been significant progress in the biochemical studies of these proteins (10, 11, 13, 14). However, many details are still elusive due to lack of three-dimensional structure. The high-resolution structure of the AHL-lactonase from BTK-AiiA, presented in this paper, fills that void. The known *Bacillus* sp. AHL-lactonases display a very high degree of amino acid sequence similarity (≈89–99%), and all of the amino acid residues implicated in catalysis, as described above, are completely conserved (Fig. 6). Previous studies on the AHL-lactonase from *Bacillus* sp. 240B1 have shown that the

enzyme is specific for acyl-substituted cyclic lactone ester (13). Although the amino acid sequence contained the ^{106}HXDH^{109} ≈ H^{169} motif, found in a number of zinc metallo-enzymes, it has been suggested on the basis of one experimental study that in the case of the AHL-lactonase, it actually represents a catalytic motif not involved in zinc or other metal binding. This has been recently contested by an independent investigation of the *B. thuringiensis* lactonase, which concluded that it is a metalloprotein containing two zinc ions (14). This study emphasized the importance of separation of active metalloprotein from inactive apoprotein during the purification procedure. Our present work shows conclusively that the AHL-lactonase contains a dinuclear Zn^{2+} center with stereochemistry and amino acid participation identical to those observed in human glyoxalase II (15) and to the bacterial RNase Z (12). The electron density map of BTK-AiiA reveals two Zn^{2+} ions with temperature factors of 22.6 Å^2 and 20.9 Å^2, when refined assuming full occupancy.

Recent studies of class B metallo-β-lactamases containing the characteristic dinuclear Zn^{2+} sites presented conflicting data on the affinities for the metal in the two sites. Five of the subclass B1 metallo-β-lactamases (i.e., BcII from *B. cereus*, BlaB from *Chryseobacterium meningosepticum*, CcrA from *B. fragilis*, IMP-1 from *Pseudomonas aeruginosa*, and VIM-2 from *P. aeruginosa*) show distinct stereochemical similarities in their active sites, with identical residues contributing to metal coordination (three histidines for Zn1 and Asp, Cys, and His for Zn2). However, the corresponding zinc affinities appear to be different, so that CcrA and IMP-1 show two high-affinity metal-binding sites, whereas BcII binds Zn1 and Zn2 with very different affinities (30). BcII is active in the presence of either one or two zinc ions, although full activity is observed when both zinc ions are bound. It has been proposed that an arginine located below the Zn2 ion in the subclass B1 β-lactamases BcII, VIM-2, and BlaB is responsible for the lower affinity (30, 31). The enzymes CcrA and IMP-1 showing high affinity for both Zn^{2+} ions have cysteine and serine, respectively, in the corresponding position. Interestingly, Arg121Cys mutation in BcII results in similar affinities for Zn1 and Zn2 (31). In BTK-AiiA, the residue occupying this position is His-109. This stereochemistry is identical to that seen in glyoxalase II (15) and RNase Z (12). Unlike the corresponding residues in subclass B1 β-lactamases, His-109 in BTK-AiiA is directly involved in binding Zn2 and is essential for BTK-AiiA activity. Thus, although we did not measure the individual Zn^{2+} affinities, BTK-AiiA is likely to have two high-affinity metal-binding sites. We anticipate that other AHL-lactonases from various bacterial sources, at least those listed in Fig. 6, may have similar metal affinities.

Note. When this paper was at the stage of revision, a similar study was published by Liu *et al.* (32). This work also described the crystal structure of an *N*-acyl-L-homoserine lactone hydrolase from *B. thuringiensis*, albeit only in the apo-form with the active site occupied by a glycerol molecule. There are no discrepancies between the two atomic models, and the conclusions regarding the enzymatic mechanism are similar. However, the structure of the complex with an inhibitory HSL molecule reported in our study allows for a more confident description of the structural roots of substrate specificity and reaction mechanism.

We thank the staff at Pohang Accelerator Laboratory (Pohang, Korea) for help with the data collection and Dr. Cheolho Yoon at the Korea Basic Science Institute for help with metal analysis. This work was funded by Molecular and Cellular BioDiscovery Research Program Grant M1-0311-00-0107 (to J.K.L.), 21C Frontier Program of Microbial Genomics and Applications Grant MG05-0401-2-0 (to C.H.L.), and the Korean Ministry of Science and Technology.

1. Parsek, M. R. & Greenberg, E. P. (2005) *Trends Microbiol.* **13,** 27–33.
2. Dong, Y. H. & Zhang, L. H. (2005) *J. Microbiol.* **43,** 101–109.
3. Zhang, L. H. (2003) *Trends Plant Sci.* **8,** 238–244.
4. Alksne, L. E. & Projan, S. J. (2000) *Curr. Opin. Biotechnol.* **11,** 625–636.
5. Otto, M. (2004) *FEMS Microbiol. Lett.* **241**, 135–141.
6. Molina, L., Rezzonico, F., Defago, G. & Duffy, B. (2005) *J. Bacteriol.* **187,** 3206–3213.
7. Zhang, R. G., Pappas, T., Brace, J. L., Miller, P. C., Oulmassov, T., Molyneaux, J. M., Anderson, J. C., Bashkin, J. K., Winans, S. C. & Joachimiak, A. (2002) *Nature* **417,** 971–974.
8. Vannini, A., Volpari, C., Gargioli, C., Muraglia, E., Cortese, R., De Francesco, R., Neddermann, P. & Marco, S. D. (2002) *EMBO J.* **21,** 4393–4401.
9. Watson, W. T., Minogue, T. D., Val, D. L., von Bodman, S. B. & Churchill, M. E. (2002) *Mol. Cell* **9,** 685–694.
10. Dong, Y. H., Xu, J. L., Li, X. Z. & Zhang, L. H. (2000) *Proc. Natl. Acad. Sci. USA* **97,** 3526–3531.
11. Lee, S. J., Park, S. Y., Lee, J. J., Yum, D. Y., Koo, B. T. & Lee, J. K. (2002) *Appl. Environ. Miocrobiol.* **68**, 3919–3924.
12. de la Sierra-Gallay, I. L., Pellegrini, O. & Condon, C. (2005) *Nature* **433,** 657–661.
13. Wang, L. H., Weng, L. X., Dong, Y. H. & Zhang, L. H. (2004) *J. Biol. Chem.* **279,** 13645–13651.
14. Thomas, P. W., Stone, E. M., Costello, A. L., Tierney, D. L. & Fast, W. (2005) *Biochemistry* **44,** 7559–7569.
15. Cameron, A. D., Ridderstrom, M., Olin, B. & Mannervik, B. (1999) *Structure Folding Des.* **7,** 1067–1078.
16. Kim, M. H., Kang, H. O., Kang, B. S., Kim, K. J., Choi, W. C., Oh, T. K., Lee, C. H. & Lee, J. K. (2005) *Biochim. Biophys. Acta* **1750,** 5–8.
17. Otwinowski, Z. & Minor, W. (1997) *Methods Enzymol.* **276,** 307–326.
18. Terwilliger, T. C. & Berendzen, J. (1999) *Acta Crystallogr. D* **55,** 849–861.
19. Terwilliger, T. C. (2000) *Acta Crystallogr. D* **56,** 965–972.
20. Jones, T. A., Zou, J. Y., Cowan, S. W. & Kjeldgaard, M. (1991) *Acta Crystallogr. A* **47,** 110–119.
21. Murshudov, G. N., Vagin, A. A. & Dodson, E. J. (1997) *Acta Crystallogr. D* **53,** 240–255.
22. Navaza, J. (1994) *Acta Crystallogr. A* **50,** 157–163.
23. Holm, L. & Sander, C. (1993) *J. Mol. Biol.* **233,** 123–138.
24. Toney, J. H., Hammond, G. G., Fitzgerald, P. M., Sharma, N., Balkovec, J. M., Rouen, G. P., Olson, S. H., Hammond, M. L., Greenlee, M. L. & Gao, Y. D. (2001) *J. Biol. Chem.* **276,** 31913–31918.
25. Harms, J. M., Schlunzen, F., Fucini, P., Bartels, H. & Yonath, A. (2004) *BMC Biol.* **2,** 1–10.
26. Ikeda, T., Kajiyama, K., Kita, T., Takiguchi, N., Kuroda, A., Kato, J. & Ohtake, H. (2001) *Chem. Lett.* **30,** 314–315.
27. Derewenda, Z. S., Lee, L. & Derewenda, U. (1995) *J. Mol. Biol.* **252,** 248–262.
28. Sarkhel, S. & Desiraju, G. R. (2004) *Proteins* **54,** 247–259.
29. Lowther, W. T., Orville, A. M., Madden, D. T., Lim, S., Rich, D. H. & Matthews, B. W. (1999) *Biochemistry* **38**, 7678–7688.
30. Davies, A. M., Rasia, R. M., Vila, A. J., Sutton, B. J. & Fabiane, S. M. (2005) *Biochemistry* **44,** 4841–4849.
31. Rasia, R. M. & Vila, A. J. (2002) *Biochemistry* **41,** 1853–1860.
32. Liu, D., Lepore, B. W., Petsko, G.A., Thomas, P. W., Stone, E. M., Fast, W. & Ringe, D. (2005) *Proc. Natl. Acad. Sci. USA* **102,** 11882–11887.